Supporting Information

Biffi et al. 10.1073/pnas.1304632110

SI Text

Nanostar Design. Star-shaped DNA supermolecules result from the self-assembly of 49-nucleotide-long base oligomers. Each structure is formed by a number of strands equal to the number of star arms (f). Oligomers forming $f = 4$ nanostars are self-assembled starting from the following four sequences:

i) 5′-CTACTATGGCGGGTGATAAAAACGGGAAGAGCATGCCCATCCACGATCG-3′

ii) 5′-GGATGGGCATGCTCTTCCCGAACTCAACTGCCTGGTGATACGACGATCG-3′

iii) 5′-CGTATCACCAGGCAGTTGAGAACATGCGAGGGTCCAATACCGACGATCG-3′

iv) 5′-CGGTATTGGACCCTCGCATGAATTTATCACCCGCCATAGTAGACGATCG-3′

The three sequences forming the $f = 3$ structures are instead:

i) 5′-CTACTATGGCGGGTGATAAAAACGGGAAGAGCATGCCCATCCACGATCG-3′

ii) 5′-GGATGGGCATGCTCTTCCCGAACTCAACTGCCTGGTGATACGACGATCG-3′

iii) 5′-CGTATCACCAGGCAGTTGAGAATTTATCACCCGCCATAGTAGACGATCG-3′

Sequences assemble as sketched in Fig. S1. Each strand is designed to bind to two other strands with two 20-nucleotide-long segments, leading to the formation of the arms of the structure. Two A bases without complementarity are placed in between the arm-forming segments to release angular constraints between the arms. Such constraints arise from the crowding of paired strands at the center of the structures. With this choice, arms are allowed some flexibility in their mutual angles. For analogous reasons, another A base with no complementary partner is added before the six-nucleotide-long overhangs; this minimizes the constraints on the mutual orientation of two bound nanostars, because each can freely rotate around the axis connecting the centers of the two structures. Despite the flexibility of the structures, electric charges on the phosphate groups will tend to keep the nanostars arms away from each other, favoring a nearly 3D tetrameric shape for the $f = 4$ structures and an open flat structure for the $f = 3$ structure.

To minimize the amount of ill-formed nanostars, we took particular care to ensure that the f distinct oligomers were present in equal stoichiometric amount in all samples. To this aim, we prepared a single starting solution by mixing the f sequences in equal ratios. The large amount of DNA involved in the starting batch and its low concentration (1 mg/mL) reduced the errors in volume and concentration measurements. The obtained homogeneous mother solution was then divided into several aliquots, which were then dried for subsequent use.

Agarose Gel Electrophoresis. To check for the actual assembly of the DNA oligomers into the desired structures, we performed electrophoretic runs under nondenaturing conditions in 3% agarose gel and Tris/borate/EDTA buffer. DNA solutions were first diluted to a concentration of ≈ 100 ng/μL maintaining the ionic strength to 48 mM NaCl, so to keep the amount of counterions about the same as in the critical samples we investigated. We ran the DNA samples in the gel at temperatures between 33 °C and 35 °C to minimize interactions between the sticky ends. The temperature could not be increased further because the agarose gel melts at 40 °C.

Electrophoretic analysis of the samples used for the experiments is shown in Fig. S2*A*. In the central lane (M), a double-strand DNA size marker (pUC8 HaeIII fragment lengths varying from 587 to 80 bp) was used to approximately gauge the position of the DNA structures. In lanes a and b we loaded a solution of $f = 4$ nanostars, and in lanes c and d we ran $f = 3$ nanostars. Lanes a and c refer to experimental samples first prepared at the critical concentration and annealed, as described in *Materials and Methods*, and later diluted as described above. The profiles of the fluorescent intensity I_F for lanes a and c, measured using a Typhoon 9200 phosphorimager and ImageQuant software (GE Healthcare) as a function of the running coordinate x, are shown in Fig. S2 *C* and *D* for $f = 4$ and $f = 3$, respectively. Each curve has been analyzed by fitting the main peak with a Gaussian curve (dashed lines) and comparing its integral (after background subtraction) with the integrated intensity of the shoulder on its right-hand side, possibly representing partially formed nanostars, smaller and thus with a larger electrophoretic mobility in the gel. In the case of $f = 4$ nanostars, such a shoulder has the shape of a wide peak and it was also approximated with a second Gaussian curve (dotted line). The shoulder in the $f = 3$ case, being instead monotonically decreasing, could not be fitted by a peak-shaped function and was thus integrated directly from the data. From this analysis we find that fully formed structures involve ∼93% of the total DNA for both $f = 3$ and $f = 4$ nanostars.

Lanes b and d in Fig. S2*A* are instead obtained by running samples from the dilute phase after centrifuging. Though the profile obtained from the dilute phase of $f = 3$ (Fig. S2*F*) is almost identical to the one of Fig. S2*D*, the dilute phase of the $f = 4$ nanostars appears to contain a large amount of ill-formed DNA structures involving approximately one-third of the total DNA. This finding suggests that upon phase separating, the system segregates in the dilute phase the largest part of misshaped structures; this is reasonable because they are typically formed by two or three strands, as indicated by their larger electrophoretic mobility, and are thus less strongly interacting with the network and more prone to evaporate out of it. This finding also offers some explanation to the fact that DNA concentration in the low-concentration side of the consolution curve is larger than expected. According to theoretical predictions, the concentration of the dilute phase well below the critical temperature should approach zero (1).

To obtain a reference value for the mobility of the different structures that could result from the partial hybridization of the oligomers, we prepared solutions in which the f sequences are progressively added. Fig. S2*B* shows such results performed with the set of sequences designed to assemble in the four-arm structure: in lane a we loaded a solution containing sequence 1 only, obtaining a unique band; in lane b we ran a mixture of sequences 1 and 2, obtaining two bands; in lane c we ran a mixture of sequences 1, 2, and 3, obtaining three bands; and in lane d we ran a mixture of sequences 1, 2, 3, and 4, obtaining four bands. Because here the stoichiometric ratios are only approximately maintained and because sequences are added sequentially with no annealing, all partial combinations are found in the solution, as desired to obtain a reference sample for the mobility of the structures. As generally expected, the mobility of the structure is reduced as its mass and its 3D complexity (2) is increased, i.e., increasing the number of arms.

Measurement of the Melting Temperature of the DNA Nanostars. DNA nanostars were designed so that the assembly of each

star would take place at a temperature significantly larger than the one at which mutual interactions occur. To check for the actual presence of such a gap in T and to properly define the annealing protocol, we characterized the melting process of our structures. Measurements were performed with a commercial instrument (LightCycler 480; Roche) that measures fluorescence emitted in the interval 483–533 nm by a saturating fluorescent dye provided with the instrument [high-resolution melting dye Master Mix (2X)]. The dye only fluoresces when bond to double-stranded DNA. As a consequence, when the dye is added to a DNA sample, its fluorescence intensity I_F is detectable only when the strands are hybridized. As T becomes larger than T_m, duplexes unbind and the fluorescence emission drops. Hence, the measurement of I_F vs. T allows us to assess the fraction of bound strands and to determine the melting temperature, defined as the temperature where half of the double helices have unbound.

To perform these measurements, samples were first annealed and diluted as described in the section *Agarose Gel Electrophoresis*, and later mixed with the tagging fluorescent dye. The results obtained with the $f=4$ nanostars are shown in Fig. S3 (red dots). In Fig. S3*A*, we plot the T dependence of the fluorescent intensity, which has the expected sigmoidal decrease as T grows. To better determine the melting temperature, we also show the derivative of I_F with respect to T (Fig. S3*B*). The melting temperature is indicated by the peak temperature. For both the $f=3$ and $f=4$ structures we find $T_m \approx 65$ °C.

With similar experiments we also checked the melting behavior of the partially built structures that we studied by gel electrophoresis in Fig. S2*B*, lanes b and c, i.e., samples containing respectively two and three of the set of four sequences to form the $f=4$ nanostars. Melting curves and derivatives for these samples are also shown in green and blue in Fig. S3. As expected, the melting temperature decreases for incomplete structures.

Analysis of the Equilibrium Critical Behavior of $f=3$ Nanostars. We extend here to the $f=3$ nanostars the kind of analysis and results described in the main text with reference only to the $f=4$ nanostars. In both systems, we measured the intensity scattered at the critical concentration at various temperatures and at various scattering angles, ranging from 30° to 152°. As discussed in the main text, we simultaneously fit the data at all investigated angles and T with the Lorentzian dependence

$$I(q)=\frac{I_L(0)}{1+q^2\xi^2}+I_{nc}. \qquad \textbf{[S1]}$$

The simultaneous best fit of the scattered intensity for all different T and q values, shown in Fig. S4 (lines), yields a robust estimates for the four fit parameters T_c, ξ_0, I_0, and I_{nc}. The resulting values for the critical temperatures (marked by a vertical line in Fig. S4) are $T_c=11.6\pm0.1$ °C and $T_c=25.5\pm0.1$ °C for $f=3$ and $f=4$, respectively. The best-fit values for ξ_0 are $\xi_0=3.2$ nm and $\xi_0=1.9$ nm for $f=3$ and $f=4$, respectively. These values are in the range of the hydrodynamic radius of the nanostar (≈ 4.5 and 4.7 nm for $f=3$ and $f=4$) and reflect the different critical density of the two systems, smaller in the case of $f=3$. Accordingly, the correlation length at the closest distance from the critical point that we explored in this study is $\xi \approx 240$ nm in the case of $f=3$ nanostars (for $T-T_c=0.3$ °C) and $\xi \approx 220$ nm in the case of $f=4$ nanostars (for $T-T_c=0.15$ °C). At these temperatures, the product ξq becomes of the order of 1 even for the measurements taken at the smallest scattering vector, indicating that in this limit the proportionality between the measured scattering intensity and the power-law divergence of the osmotic compressibility (strictly valid only for $q\to 0$) becomes unobservable.

Further Discussion About Critical Slowing Down and Activated Dynamics. The analysis of the dynamic light-scattering data indicates that the critical fluctuations giving rise to the scattering divergence decay through the slow process. Because the interactions of DNA structures involve short-ranged on/off bonds, it is possible to describe the formation and dissipation of concentration fluctuations by distinguishing two families of contributing processes: those that involve the breaking of interstructure bonds and those that do not. The latter include the diffusion of unbound structures (or small aggregates of structures), accounting for the relaxation of the intensity correlation function at high T; they also include bond-preserving oscillations of the network, expected to contribute to the dynamics as the network grows (3). We could not, however, detect convincing clues of the presence of such network oscillations. Indeed, as T is decreased, network oscillations should increase in amplitude together with the scattering from the network, but they should not show an Arrhenius growth as the slow components do. For these reasons, network oscillations should give rise to kinetic contributions having a behavior different from either the observed fast and slow components. Data thus suggest that bond-maintaining network oscillations might be of small relevance and buried under the other phenomena more easily detectable.

Overall, bond-preserving mechanisms provide a partial decorrelation, limited by the constraints imposed by the topology of the network, because only by breaking bonds can the system become fully ergodic; the local disruption of network bonds enables its readjustment into different patterns. This process can take place either through nanostars "evaporating" away from the network and reconnecting elsewhere or through the rearrangements of network portions made flexible by the opening of bonds. The kinetics of this process are intrinsically limited by the rate of unbinding events and thus necessarily slower than the free diffusion of the structures, being the lifetime of short-paired oligonucleotides easily spanning into the millisecond regime (4).

Thus, the analysis of the activated slowing down consistently indicates that to achieve ergodicity, the system undergoes readjustments that involve the breaking of a number of bonds lower than f. This notion makes good physical sense because breaking events take place more probably where the network is weakest, and less probably involve the disconnection of fully bonded supermolecules.

A striking result presented in the main text is that the slow decay does not show the power-law divergence expected for the critical slowing down. It is interesting to evaluate what would be the T dependence of the correlation time expected for an "ordinary" phase transition on the basis of the critical slowing down for the 3D Ising model with conserved order parameter. For $q\to 0$, $\tau_T=\tau_{T,0}\ \xi^z$, where $\tau_{T,0}$ is a coefficient and $z=2$ is the critical exponent for the dynamics scaling of the 3D Ising system (5).

We display in Fig. S5 the predicted $\tau(T)$ with the $\tau_{T,0}$ coefficient chosen so to match the measured τ at high T, where the dynamics is purely diffusive. Quite evidently, the expected slowing down is, in the explored T range, much less significant than the one observed. Only very close to T_c the predicted τ_T would become slower than the measured τ. This simple estimate suggests that in the whole T range here explored, the critical slowing down is buried under the steep Arrhenius–Eyring dependence describing the growing stickiness of the DNA nanostars. We cannot exclude also the possibility that the finite q of our measurements can also contribute to mask the power-law divergence of the characteristic time, similar to what has been observed for the scattered intensity.

Estimate of the Free Energies and Melting Temperature Based on Database Values. A large number of studies have been devoted to introduce simple approaches enabling one to compute the variation in Gibbs free energy G involved in the formation of duplexes

from DNA single strands. The formation of a DNA duplex involves variations of both enthalpy (H) and entropy (S), arising from a multiplicity of sources, which include conformational changes of the strands, solvent reorientation, and ion redistributions. A diffuse approach to evaluate ΔG is the so-called "nearest neighbor" (NN) model (6, 7). According to such a model, ΔG of a duplex involving N paired bases is calculated as a sum of various contributions: (*i*) $N-1$ "quadruplet" contributions ΔG_Q, each quadruplet being formed by two consecutive nucleotides on one strand and the corresponding nucleotides on the other strand. Fig. S6 shows a drawing of two paired overhangs with the sequence used in our experiments. In the same figure, the quadruplets are marked by dashed lines; (*ii*) an "initiation" ΔG_{INIT}, representing the free energy cost involved in constraining the two strands in the conformational space available to them when they are bonded in the absence of the contributions from pairing and stacking (8).

The specific value for ΔG_Q, and of both its components ΔH_Q and ΔS_Q, depends on the specific bases involved in the quadruplets. Analysis of the database of DNA thermodynamic behavior has allowed for determining such values. By adopting the values for ΔH_Q and ΔS_Q listed in ref. 6, we determine the enthalpy and entropy involved in the hybridization of the overhangs providing the interaction energy between the DNA structures. By summing up all quadruplet contributions (listed among parenthesis), one finds $\Delta H(CGATCG)=\sum_{N-1}\Delta H_Q+\Delta H_{INIT}=(-10.6-8.2-7.2-8.2-10.6+0.2)$ kcal/mol $=-44.6$ kcal/mol and $\Delta S(CGATCG)=\sum_{N-1}\Delta S_Q+\Delta S_{INIT}+\Delta S_{SALT}=(-27.2-22.2-20.4-22.2-27.2-5.7-6.7)$ cal/(mol K) $=-132$ cal/(mol K). The term ΔS_{SALT} compensates for the fact that tabulated values refer to 1 M NaCl, whereas our experiments were performed at a total of 48 mM (6).

The hybridization energy and enthalpy estimates enable us to predict the melting temperature T_m of the duplexes, i.e., the T at which half of the duplexes are unbound. Indeed, the T_m of the overhangs is a crucial parameter in designing the structures and in particular in determining the length of the overhangs. When dealing with self-complementary sequences, as the 6 mer forming the overhangs, T_m can be expressed as $\frac{1}{T_m}=\frac{R}{\Delta H}ln(f[c])+\frac{\Delta S}{\Delta H}$, where $[c]$ is the molar concentration of the DNA nanostars (9). At the critical isochore, when $f=4$, this evaluation leads to $T_m\approx 30.5$ °C. In the case of $f=3$, the smaller f and $[c]$ values bring $T_m=26.7$ °C. At T_m, a large fraction (half) of the overhangs are duplexed, i.e., a situation where DNA nanostars are strongly interacting. Actually, nanostars interactions start becoming relevant at a larger T, as indicated by the appearance of the slower decay in the correlation curves (Fig. 3*A*). By adopting a similar approach, we can estimate the temperature T_b introduced in the main text, defined as the temperature at which 10% of the overhangs are duplexed. For $f=4$, $T_b\approx 42.4$ °C.

One property of the DNA nanostars that has made our investigation successful is the relatively small difference between the critical temperatures of the $f=3$ and $f=4$ systems, which enabled us to explore both phase diagrams in a limited T range. Given the significant difference in binding energy of the two structures at a given T—their ratio being of the order of 3/4—one could expect a corresponding large difference (of the order of 30%) in the critical temperatures. We find instead a difference in T_c of ∼5%. This behavior is easily understood on the basis of the large entropic component in the binding free energy between nanostars, which produces a large free-energy variation over a narrow T range. By using the quantities determined above, we obtain, at the two critical temperatures, $\Delta G(T=11.6\ ^{\circ}\mathrm{C})\approx -7.0\pm 0.1$ kcal/mol and $\Delta G(T=25.5\ ^{\circ}\mathrm{C})\approx -5.2\pm 0.1$ kcal/mol. The ratio between these values is $0.74\sim 3/4$. The comparison between the energy involved in the two systems at their critical point can be made more accurate on the basis of average number of bonds of each nanostar at T_c. Computer simulation of low-valency systems has consistently indicated that, at the critical point, the number of bonds per particle is 2.1 for $f=3$ and 2.6 for $f=4$ (10). The total bond energy per particle is thus 2.1 $\Delta G(T=11.6\ ^{\circ}\mathrm{C})$ for $f=3$ nanostars and 2.6 $\Delta G(T=25.5\ ^{\circ}\mathrm{C})$ for $f=4$ nanostars. These two values are both ≈ -14 kcal/mol, corresponding to ∼23 k_BT per nanostar.

Estimate of the Concentration of Fully Bond Networks. Our data indicate that the dense phase at coexistence of $f=3$ and $f=4$ DNA nanostars have markedly different concentration. This result agrees with what predicted in ref. 1 on the basis of Wertheim thermodynamics perturbation theory.

Here we provide a simplified argument to estimate the density of fully bonded networks formed by DNA nanostars of valence f, i.e., networks in which all of the arm tips are bound to neighboring nanostars. Although such a network does not need to have a regular structure, the simplest strategy to estimate concentrations is to assume that the nanostars are arranged in a regular lattice.

We thus assume that $f=4$ nanostars are ordered like a diamond lattice. We also assume that the distance between the centers of bonded nanostars is 17 nm, which correspond to the length obtained when the arms joined in a bond and the duplex formed by the paired overhangs are all perfectly straight and aligned in a line. From the structure of the diamond lattice we deduce that such a network would have a density of 0.22 mM, corresponding to a DNA concentration of 13.3 mg/mL.

In the case of $f=3$ nanostars, there is not an obvious lattice to refer to. However, we can modify the diamond lattice by replacing every $f=4$ nanostar with two $f=3$ nanostars connected through one bond. Taken together, such a pair of $f=3$ nanostars makes one structure with a valence equal to 4. Given the angular flexibility of the arms in the structures we explore, we can assume that the angles between the four open arms of the coupled trimers equal the tetrahedral angle (∼109.5°). Hence, by taking the diamond lattice and replacing each valence-4 atoms with doublets of connected valence-3 atoms, all doublets equally oriented along one of the axes of the cubic unit cell, we obtain a different crystalline structure. By adopting the same center-to-center distance for bonded $f=3$ nanostars, we obtain that such a crystal would have a density of 16 mM, corresponding to a DNA concentration of 7.3 mg/mL.

These figures are lower bound estimates, because any bending or fluctuation of the bonded nanostar arms reduces their distance and thus increases the concentration.

1. Bianchi E, Largo J, Tartaglia P, Zaccarelli E, Sciortino F (2006) Phase diagram of patchy colloids: towards empty liquids. *Phys Rev Lett* 97(16):168301–168304.
2. Stewart KM, McLaughlin LW (2004) Four-arm oligonucleotide Ni(II)-cyclam-centered complexes as precursors for the generation of supramolecular periodic assemblies. *J Am Chem Soc* 126(7):2050–2057.
3. Krall AH, Weitz DA (1998) Internal dynamics and elasticity of fractal colloidal gels. *Phys Rev Lett* 80(4):778–781.
4. Howorka S, Movileanu L, Braha O, Bayley H (2001) Kinetics of duplex formation for individual DNA strands within a single protein nanopore. *Proc Natl Acad Sci USA* 98(23):12996–13001.
5. Coniglio A, Klein W (1980) Clusters and Ising critical droplets: A renormalisation group approach. *J Phys A* 13(8):2775.
6. SantaLucia J, Jr., Hicks D (2004) The thermodynamics of DNA structural motifs. *Annu Rev Biophys Biomol Struct* 33:415–440.
7. Bellini T, Cerbino R, Zanchetta G (2012) DNA-based soft phases. *Top Curr Chem* 318: 225–279.
8. Manyanga F, et al. (2009) Origins of the "nucleation" free energy in the hybridization thermodynamics of short duplex DNA. *J Phys Chem B* 113(9):2556–2563.
9. Owczarzy R, et al. (1997) Predicting sequence-dependent melting stability of short duplex DNA oligomers. *Biopolymers* 44(3):217–239.
10. Foffi G, Sciortino F (2007) On the possibility of extending the Noro-Frenkel generalized law of correspondent states to nonisotropic patchy interactions. *J Phys Chem B* 111(33):9702–9705.

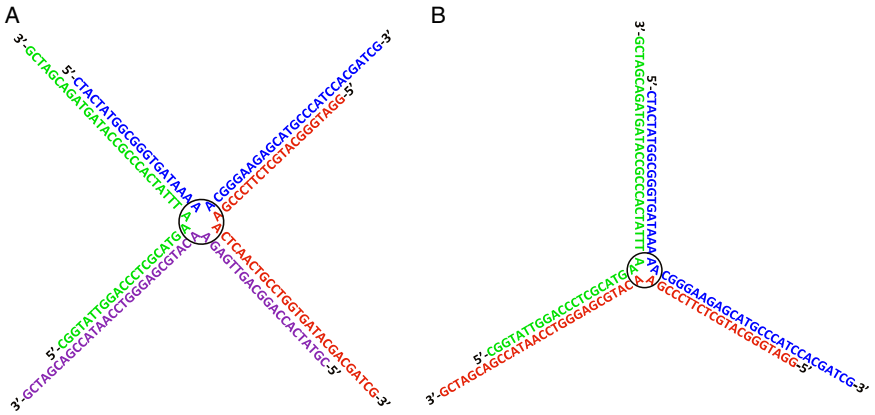

Fig. S1. Schematic representation of the pairing of the DNA sequences in (*A*) $f = 4$ and (*B*) $f = 3$ nanostars.

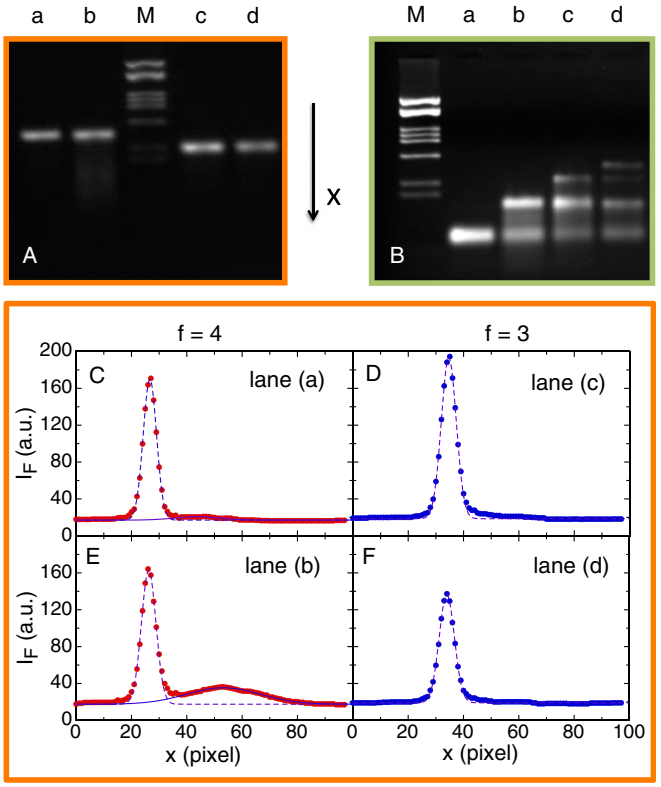

Fig. S2. Electrophoretic measurements on 3% agarose gel. (*A*) Gel runs of samples with properly balanced stoichiometric ratios. Lanes a and b: $f = 4$ nanostars. Lanes c and d: $f = 3$ nanostars. Lanes a and c: critical concentration. Lanes b and d: dilute phases extracted from the capillaries after centrifugation. Lane M shows the bands of reference sequences. (*B*) Gel runs of partially formed $f = 4$ nanostars. The solution in lane a contains only sequence 1 of the four sequences forming the structures; lane b contains sequences 1 + 2; lane c sequences 1 + 2 + 3; lane d sequences 1 + 2 + 3 + 4. In these samples, stoichiometric ratios were not precise, and the samples were not annealed, resulting in multiple bands. (*C–F*) Intensity profiles extracted from the four lanes of the gel in *A* as a function of the pixel position.

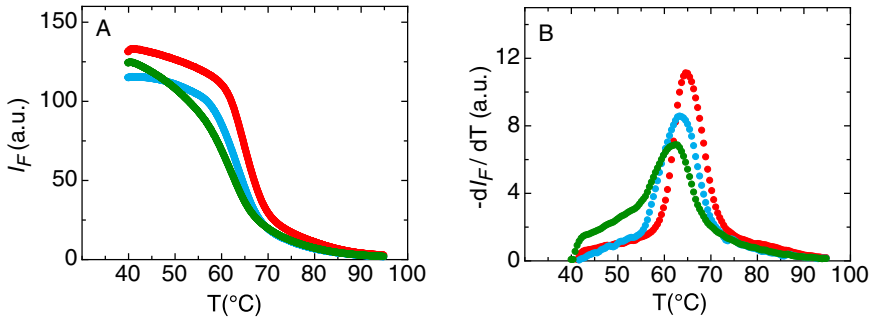

Fig. S3. Melting curves as measured by the fluorescent emission of a fluorochrome whose emission vanishes when DNA double-strands unbind. (*A*) Fluorescence emission vs. temperature for fully formed $f = 4$ nanostars (red dots) and for partially formed $f = 4$ nanostars, made by two and three of the four building strands (green and blue dots, respectively). (*B*) Inverse derivative of the fluorescence intensity vs. temperature.

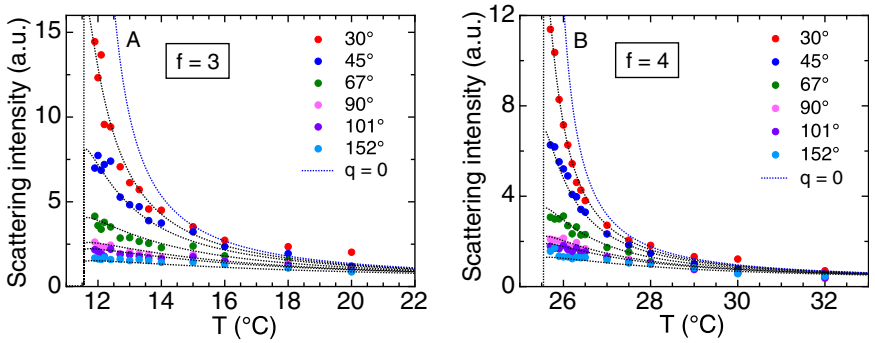

Fig. S4. Scattered intensity by solutions of (*A*) $f = 3$ and (*B*) $f = 4$ nanostars prepared at the critical concentration. Lines represent the best fit obtained by fitting simultaneously the whole set of data of each system by Eq. **1**. Vertical lines mark the critical temperatures. The scattering angles, and the corresponding scattering vectors explored in this experiment, are 30° (q = 8.15 μm^{-1}), 45° (q = 12.1 μm^{-1}), 68° (q = 17.6 μm^{-1}), 90° (q = 22.3 μm^{-1}), 101° (q = 24.3 μm^{-1}), and 152° (q = 30.6 μm^{-1}).

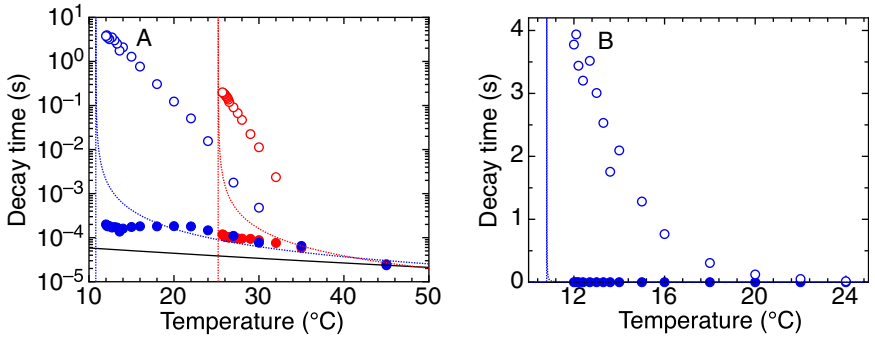

Fig. S5. (*A*) Comparison between data and expected critical slowing down for both the $f = 3$ and $f = 4$ systems. (*B*) Linear plot of the same data, limited to the region of interest for the $f = 3$ structures.

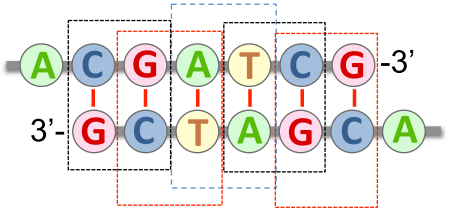

Fig. S6. Sketch of two mutually paired structure overhangs having sequence CGATCG and attached to the structure arms via an unpaired A base. Dashed boxes mark the five quadruplets used to estimate the hybridization free energy.